
Graphene Nanocomposites

Mingchao Wang, Cheng Yan and Lin Ma

Additional information is available at the end of the chapter

<http://dx.doi.org/10.5772/50840>

1. Introduction

Graphene, one of the allotropes (diamond, carbon nanotube, and fullerene) of carbon, is a monolayer of honeycomb lattice of carbon atoms discovered in 2004. The Nobel Prize in Physics 2010 was awarded to Andre Geim and Konstantin Novoselov for their ground breaking experiments on the two-dimensional graphene [1]. Since its discovery, the research communities have shown a lot of interest in this novel material owing to its unique properties. As shown in Figure 1, the number of publications on graphene has dramatically increased in recent years. It has been confirmed that graphene possesses very peculiar electrical properties such as anomalous quantum hall effect, and high electron mobility at room temperature ($250000 \text{ cm}^2/\text{Vs}$). Graphene is also one of the stiffest (modulus $\sim 1 \text{ TPa}$) and strongest (strength $\sim 100 \text{ GPa}$) materials. In addition, it has exceptional thermal conductivity ($5000 \text{ Wm}^{-1}\text{K}^{-1}$). Based on these exceptional properties, graphene has found its applications in various fields such as field effect devices, sensors, electrodes, solar cells, energy storage devices and nanocomposites. Only adding 1 volume per cent graphene into polymer (e.g. polystyrene), the nanocomposite has a conductivity of $\sim 0.1 \text{ Sm}^{-1}$ [2], sufficient for many electrical applications. Significant improvement in strength, fracture toughness and fatigue strength has also been achieved in these nanocomposites [3-5]. Therefore, graphene-polymer nanocomposites have demonstrated a great potential to serve as next generation functional or structural materials.

Relatively, limited research has been conducted to understand the intrinsic structure-property relationship in graphene based composites such as graphene-polymer nanocomposites. The mechanical property enhancement observed in graphene-polymer nanocomposites is generally attributed to the high specific surface area, excellent mechanical properties of graphene, and its capacity to deflect crack growth in a far more effectively way than one-dimensional (e.g. nanotube) and zero-dimensional (e.g. nanoparticle) fillers [5]. On the other hand, the graphene sheets or thin platelets dispersed in polymer matrix may create wavy or wrinkled structures that tend to unfold rather than stretch under applied loading.

This may severely reduce their stiffness due to weak adhesion at the graphene-polymer interfaces [6]. However, a wrinkled surface texture could create mechanical interlocking and load transfer between graphene and polymer matrix, leading to improved mechanical strength [7]. Furthermore, structural defects and stability of graphene can significantly influence the graphene-polymer interfacial behaviour. Therefore, further work is required to understand the structure-property relationship in graphene and the graphene-polymer interface behaviour.

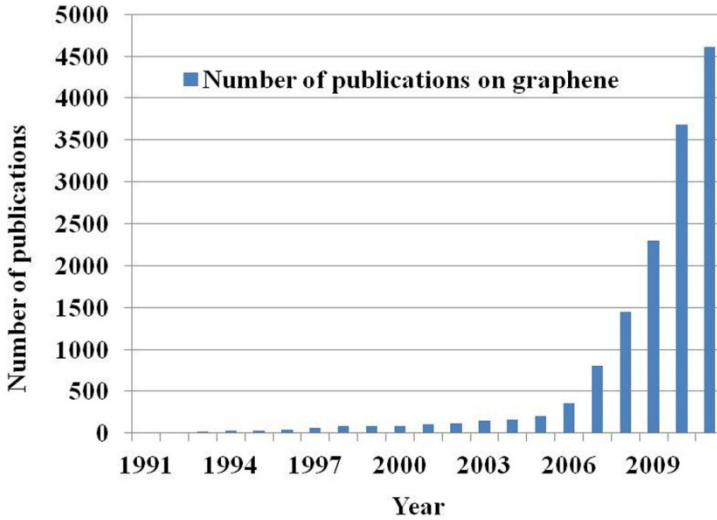


Figure 1. Number of publications on graphene in past 20 years.

2. Graphene

2.1. Mechanical and electrical properties

Mechanical properties

Graphene, a special monolayer of hexagon-lattice, are even stiffer and stronger than carbon nanotube (CNT). By nanoindentation on a free-standing monolayer graphene, the Young's modulus and intrinsic strength were estimated as ~ 1.0 TPa and $\sigma_{int}=130$ GPa at a strain of $\epsilon_{int}=0.25$ [8,9]. Atomistic simulations demonstrated size and chirality dependent elastic properties in graphene nanoribbons [10,11]. The size effect on Young's modulus is negligible when the diagonal length of a graphene nanoribbon is over 10.0 nm. The maximum Cauchy (true) stress and fracture strain for graphene loaded in the armchair direction were estimated as 102 GPa and 0.13, respectively. Higher values were observed in the zigzag direction, i.e., 129 GPa and 0.20, respectively. Besides size and chirality dependence, temperature also shows significant influence on the mechanical properties of graphene. Zhao et al. suggested[12] that Young's modulus does not vary significantly with temperature until

about 1200 K, beyond which graphene becomes softer. The fracture strength and fracture strain decrease significantly with the increase with temperature [12]. Even though monolayer graphene is generally regarded as an ideal structure for practical applications, graphene flakes with few layers are often present in the routine of synthesis, such as mechanical exfoliation. It has been confirmed the layer number is another noticeable factor in dictating the mechanical properties. Table 1 summarizes the intrinsic mechanical properties of the single, bilayer and trilayer graphene.

Method	Material	Mechanical properties	References
AFM	Monolayer graphene	$E = 1 \pm 0.1$ TPa	[8]
		$\sigma_{\text{int}} = 130 \pm 10$ GPa at $\epsilon_{\text{int}} = 0.25$	
Raman	Graphene	Strain $\sim 1.3\%$ in tension	[13]
		Strain $\sim 0.7\%$ in compression	
AFM	Monolayer	$E = 1.02$ TPa; $\sigma = 130$ GPa	[14]
	Bilayer	$E = 1.04$ TPa; $\sigma = 126$ GPa	
	Trilayer graphene	$E = 0.98$ TPa; $\sigma = 101$ GPa	

Table 1. Mechanical properties of graphene.

In a single graphene sheet, the sp^2 hybridized carbon atoms are arranged in hexagonal fashion. A single hexagonal ring comprises of three strong in-plane sigma bonds p_z orbitals perpendicular to the planes. Different graphene layers are bonded by weak p_z interaction. As a result, the hexagonal structure is generally stable but delamination can occur between the graphene layers when subjected to shear stresses. For example, scotch tape was used to obtain single graphene sheet by peeling bulk graphite layer by layer [1]. In general, the interaction between graphene and other material is considered to be in the form of non-bonded van der Waals attraction. For example, the graphene-SiO₂ adhesion energy estimated by pressurized blister tests is about 0.45 ± 0.02 Jm⁻² for monolayer graphene and 0.31 ± 0.03 Jm⁻² for two- to five-layer graphene sheets [15]. These values are greater than the adhesion energies measured in typical micromechanical structures and are comparable to solid-liquid adhesion energies. This can be attributed to the extreme flexibility of graphene, which allows it to conform to the topography of even the smoothest substrates, thus making its interaction with the substrate more liquid-like rather than solid-like.

Electrical transport properties

As a semiconductor with zero band gap, graphene has unusual charge carriers that behave as massless relativistic particles (Dirac fermions), which is different from electrons when subjected to magnetic fields and has the anomalous integer quantum Hall Effect (QHE) [16]. This effect was even observed at room temperature [17]. The band structure of single layer graphene exhibits two bands which intersect at two inequivalent point K and K₀ in the reciprocal space. Near these points electronic dispersion resembles that of the relativistic Dirac electrons. K and K₀ are referred as Dirac points where valence and conduction bands are degenerated, making graphene a zero band gap semiconductor.

Another important characteristic of single-layer graphene is its ambipolar electric field effect at room temperature, which is charge carriers can be tuned between electrons and holes by applying a required gate voltage [1,18]. In positive gate bias the Fermi level rises above the Dirac point, which promotes electrons populating into conduction band, whereas in negative gate bias the Fermi level drops below the Dirac point promoting the holes in valence band.

2.2. Structural defect

Recently, different synthesis methods have been developed to produce high quality graphene such as chemical vapor-deposition (CVD)[19-21] and epitaxial growth[22,23] on metal or SiC substrates. However, various defects and impurities are often introduced into graphene during the processing. The second law of thermodynamics also indicates the presence of a certain amount of disorder in crystalline materials. Like other crystalline materials, it is expected the defects and impurities may strongly influence the electrical, mechanical and thermal properties of graphene. Structural defects, such as Stone-Wales (S-W) defect and vacancies in graphene, can significantly reduce its intrinsic strength. Quantized fracture mechanics (QFM) as well as molecular dynamics (MD) simulations demonstrated that even one vacancy can lead to strength loss by 20% of pristine graphene [11]. Zheng et al. [24] found that Young's modulus depends largely on the degree of functionalization and molecular structure of the functional groups attached to a graphene sheet, attributed to the binding energy between the functional groups and the graphene, as well as sp^2 -to- sp^3 bond transition. This was also confirmed in the graphene with hydrogen function groups [25].

On the other hand, imperfection in graphene can be used to tailor the properties of graphene and achieve new functions[26,27]. Defects in graphene are divided into two different types, namely *intrinsic* and *extrinsic*. Imperfection without the presence of foreign atoms is referred to as intrinsic type, and other is referred to as extrinsic type. In terms of dimensionality, defects in graphene can also be categorized as point defect (0D) and line defect (1D). In this section, we will review the formation of several typical *intrinsic* lattice defects in graphene.

Point defects

One of the unique properties of graphene is its ability to reconstruct the atom arrangement by forming non-hexagonal rings. The simplest example is SW defect [28], which does not involve any removed or added atoms. Four hexagons are transformed into two pentagons and two heptagons [SW(55-77) defect] by rotating one C-C bond by 90° . The existing SW defect was observed in recent experimental research [29], as shown in Figure 2a. The estimated formation energy (E_f) for SW(55-77) defect is 5eV by density functional theory (DFT) calculation [30,31], and 20 eV by molecular dynamics (MD) simulation [11]. Besides these atomic simulations, a topological continuum framework was proposed to evaluate the formation energy of associated and dissociated SW defects in graphene [32]. The high formation energy indicates a negligible kinetic formation rate of SW defect below 1000 °C. In addition, it has been reported that low mechanical strain (less than failure strain) cannot lead to the formation of SW defects [11].

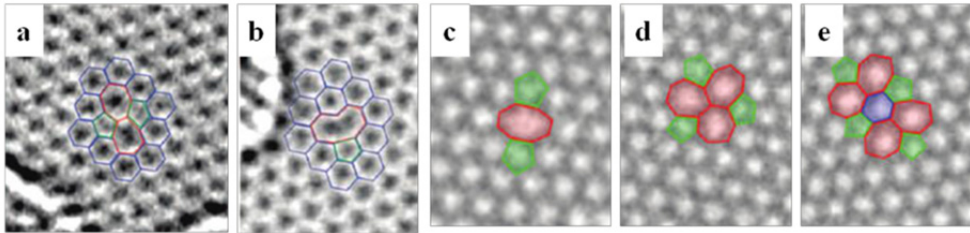


Figure 2. (a) Stone-Wales (SW55-77) defect, (b) Single vacancy (SV) defect ([29]. Reprinted with permission from American Chemical Society, Copyright 2008), (c) double vacancies (DV5-8-5), (d) double vacancies (DV555-777), (e) double vacancies (DV5555-6-7777) defect (Reprinted with permission from Ref [37] Copyright 2010 American Chemical Society).

Besides SW defect, another simple defect in graphene is missing lattice atoms. Single vacancy (SV) in graphene was experimentally observed using TEM [29,33] and scanning tunneling microscope (STM) [34]. As shown in Figure 2b, one dangling bond remains toward the missing atom, which leads to the formation of a five-member ring and a nine-member ring. Such SV defect has formation energy $E_f \approx 7.5$ eV [35], which is much higher than that in many other materials (i.e. less than 3.0 eV in most metals). Double vacancies (DV) can also be created either by the combination of two SVs or by removing two neighbouring atoms. As shown in Figure 2c, two pentagons and one octagon (DV(5-8-5) defect) appear instead of four hexagons. Simulations [35] show that the formation energy of a DV (about 8 eV) is of the same order for a SV. In fact, the DV(5-8-5) is not even the energetically favoured one. There are also other possible ways for a graphene lattice to arrange two missing atoms. For example, one C-C bond in the octagon of DV(5-8-5) defect transforms it into three pentagons and three heptagons (DV(555-777) defect) (Figure 2d). After rotating another C-C bond, DV (555-777) defect is transformed into DV(5555-6-7777) defect (Figure 2e). Multiple vacancies (MV) are created by removing more than 2 atoms. Generally, DV with even number of missing atoms are energetically favoured than that with odd number of missing atoms, where a dangling bond exists in the vicinity of defect [36].

Line defects

One-dimensional line defects have been observed in recent experimental studies [27,38,39]. Generally, these line defects have tilted boundaries separating two domains of different lattice orientations [37]. For example, a domain boundary has been observed to appear due to lattice mismatch in graphene grown on a Ni surface [27]. It is well-known that the properties of polycrystalline materials are governed by the size of grains as well as the atomic structure of grain boundaries, especially in two-dimensional graphene. In particular, grain boundaries may dominate the electronic transport in graphene [40].

2.3. Morphology

Generally, it is believed that long-range order does not exist according to Mermin-Wagner theorem [41]. Thus, dislocation should appear in 2D crystals at any finite temperature.

However, over the past two decades, researchers have demonstrated that long-range order can present due to anharmonic coupling between bending and stretching modes [42,43]. As a result, 2D membranes can exist but tend to be rippled. The typical height of roughness fluctuation scales with sample size L as L^ξ , with $\xi \approx 0.6$. Indeed, ripples in freestanding graphene were observed in recent experiments [44,45]. This kind of geometrical feature is generally referred as *intrinsic* morphology. In contrast, the morphology of substrate-supported graphene is regulated by the graphene-substrate interaction and is referred as *extrinsic* morphology. In this section, both *intrinsic* and *extrinsic* morphologies of graphene are reviewed.

Intrinsic morphology

As mentioned above, the shape of 2D graphene in 3D space is affected by its random intrinsic corrugations. The out-of-plane corrugations lead to increased strain energy but stabilize the random thermal fluctuation [46]. TEM observation indicates that suspended graphene sheets are generally not flat and the surface roughness can reach to about 1 nm [44]. In atomic force microscopy (AFM) measurements, nanometre-high buckles were observed in a single layer of graphene. The buckles in multi-layer graphene can penetrate from one layer to another [45]. To verify the experimental observation, simulations has been conducted to investigate the morphology of graphene and good agreement with the experiment has been achieved [47,48]. Atomistic Monte Carlo simulations also indicates that thermal fluctuation can create ripples with a ridge length around 8 nm [47], which is compatible with experimental findings (5-10 nm) [44].

Besides the effect of thermal fluctuation, sample size, aspect ratio, free edges and structural defects can also significantly affect the intrinsic morphologies of graphene. The constraint condition at the edge (e.g. periodic boundary or open edge) also affects the out-of-plane displacement [49]. As the aspect ratio (n) increases, its morphology changes from planar membrane, worm-like nanoribbons, and above the critical value $n_{cr}=50$, the nanoribbons self-fold into nanoscrolls, forming another structural phase, as shown in Figure 3. This implies that low aspect ratio in graphene nanoribbons is preferred for electronic applications as self-folding can be avoided.

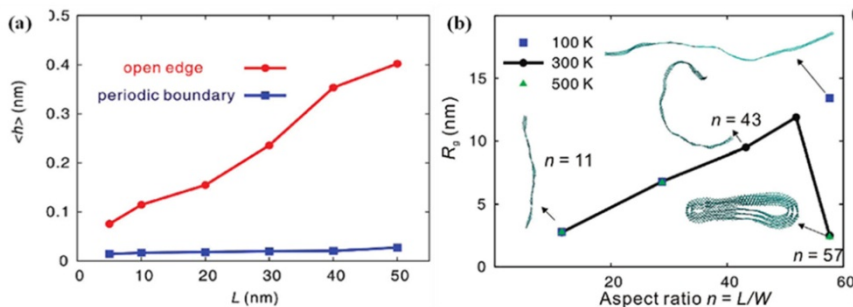


Figure 3. (a) Averaged out-of-plane displacement amplitude $\langle h \rangle$ of both graphene sheets with periodic boundary condition (red line) and open edges (blue line), and (b) Dependence of graphene sheet conformation on aspect ratio $n=L/W$ (Reprinted with permission from Ref. [49] Copyright 2010 American Chemical Society).

For finite-sized graphene with open edges, the reconstruction of free edges results in non-zero edge stress. For regular (armchair and zigzag) and reconstructed edges terminated with hydrogen (r-H edge), they are subjected to compressive stresses [50-52]. Corresponding to the compressive stress, out-of-plane ripples are primarily confined to the edge areas. The influence of edge stresses is more dramatic in the nanoribbons than that in the sheets. Tensile stress is often associated with reconstructed edges terminated with pentagons-hexagons ring (r-5-6 edge) and pentagons-heptagons ring (r-5-7 edge)[53]. Such edge stress leads to large-scale curling of graphene sheets into cylindrical surfaces with their ends arching inward. Furthermore, attached chemical groups on graphene surface can change its morphology as a result of bond transition from sp^2 type to sp^3 type [54].

Extrinsic morphology

Graphene is also found to appear corrugations when fabricated on a substrate, which is often referred as the intrinsic morphology of graphene. Recent experiments indicate that unwanted photo-resist residue under the graphene can lead to such random corrugations. After removal of the resist residue, atomic-resolution images of graphene show that the graphene corrugations stem from its partial conformation to its substrate [55]. In addition, it has been demonstrated that single and few-layer graphene partially follow the surface morphology of the substrates [56-58]. These experimental studies suggest that the regulated extrinsic morphology of substrate-supported graphene is essentially different from that of free-standing graphene.

In terms of energy, the extrinsic morphology of graphene regulated by the supporting substrate is governed by the interplay among three types of energetics: (1) graphene strain energy, (2) graphene-substrate interaction energy and (3) substrate strain energy [46]. As graphene conforms to a substrate, the strain energy in the graphene and substrate increases but the graphene-substrate interaction energy decreases. By minimizing the total energy of the system, the equilibrium extrinsic morphology can be determined. In practice, the underlying substrate can be patterned with different features such as nanowires (1D), nanotubes (1D) or nanoparticles (0D). Graphene on a patterned substrate will conform to a regular extrinsic morphology.

For the substrate with 1D periodic sinusoidal surface, the regulated graphene is expected to have a similar morphology that can be described by

$$w_g(x) = A_g \cos\left(\frac{2\pi x}{\lambda}\right), \quad w_s(x) = A_s \cos\left(\frac{2\pi x}{\lambda}\right) - h \quad (1)$$

where λ is the wavelength; h is the distance between the middle planes of the graphene and the substrate surface; A_g and A_s are the amplitudes of the graphene morphology and the substrate surface, respectively. The graphene-substrate interaction energy is given by summing up all interaction energies between carbon and the substrate atoms via van der Waals force, i.e., [59]

$$E_{\text{int}} = \int_S \int_{V_s} V(r) \rho_S dV_S \rho_C dS \quad (2)$$

The strain energy of graphene sheet is given by

$$E_s = \frac{1}{\lambda/2} \int_0^{\lambda/2} \frac{D}{2} \left(\frac{\partial^2 w_s}{\partial x^2} \right)^2 dx = \frac{4\pi^4 D A_s^2}{\lambda^4} \quad (3)$$

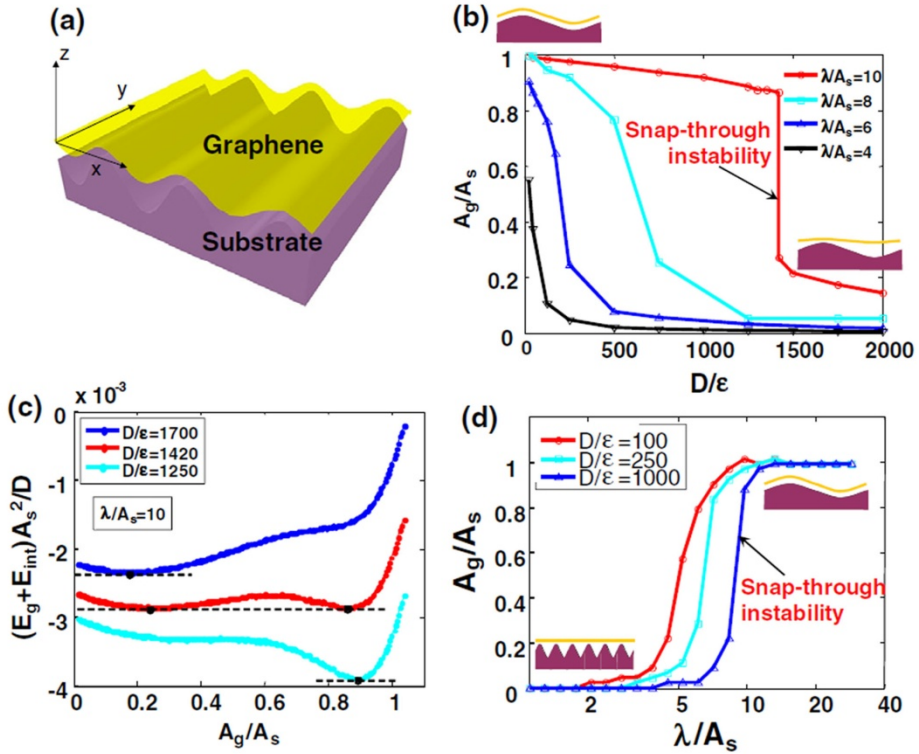


Figure 4. (a) Schematics of a graphene sheet on the corrugated substrate. (b) and (d) The normalized equilibrium amplitude of the graphene corrugation A_g/A_s as a function of D/ϵ for various λ/A_s . (c) Normalized total energy as a function of A_g/A_s for various D/ϵ (Reprinted with permission from Ref. [59] Copyright 2010 IOP Publishing).

In terms of the minimum potential energy, there exists a minimum value of $(E_g + E_s)$ where A_g and h define the equilibrium morphology of the graphene on the substrate. Figure 4 shows the normalized equilibrium amplitude of the graphene corrugation A_g/A_s as a function of D/ϵ for various λ/A_s . By analysing given substrate surface roughness (λ/A_s) and graphene-substrate interfacial bonding (D/ϵ) respectively, it was found that there is a sharp transition in the normalized equilibrium amplitude of the graphene corrugation. Such snap-through instability of the extrinsic morphology of graphene on the substrate can be understood by the energetic parameter shown in Figure 4c. Besides the interfacial bonding energy, the substrate surface roughness can also influence the extrinsic morphology graphene, as

shown in Figure 4d. Similar to the effect of substrate on the morphology of mounted graphene, 0D and 1D patterned nanoscale array can determine the equilibrium extrinsic morphology of graphene on the substrate [60,61].

3. Graphene-polymer nanocomposites

Polymer matrix nanocomposites with graphene and its derivatives as fillers have shown a great potential for various important applications, such as electronics, green energy, aerospace and automotive industries. As mentioned before, 2-D graphene possesses better electrical, mechanical and thermal properties as well as other unique features, including higher aspect ratio and larger specific surface area as compared to other reinforcements such as CNTs and carbon and Kevlar fibres. It is reasonable to expect some significant improvement in a range of properties in the composites with graphene as nanofiller. The recent success in synthesis of large amount of graphene further promotes the development of graphene based composite and hybrid materials.

3.1. Synthesis of graphene-polymer nanocomposites

Similar to processing other polymer matrix composites, solution blending, melt mixing and in-situ polymerization are the commonly used approaches to produce graphene-polymer composites.

Solution blending

Solution blending is the most popular technique to fabricate polymer-based composites in that the polymer is readily soluble in common aqueous and organic solvents, such as water, acetone, dimethylformamide (DMF), chloroform, dichloromethane (DCM) and toluene. This technique includes the solubilisation of the polymer in suitable solvents, and mixing with the solution of the dispersed suspension of graphene or graphene oxide (GO) platelets. The polymers including PS [2], polycarbonate [62], polyacrylamide, polyimides [63] and poly(methyl methacrylate) (PMMA) [64] have been successfully mixed with GO in solution blending where the GO surface was usually functionalized using isocyanates, alkylamine and alkyl-chlorosilanes to enhance its dispersability in organic solvents. In addition, the facile production of aqueous GO platelet suspensions via sonication makes this technique particularly appealing for water-soluble polymers such as poly(vinyl alcohol) (PVA) [65] and poly(allylamine), composites of which can be produced via simple filtration [65].

For solution blending methods, the extent of exfoliation of GO platelets usually governs the dispersion of GO platelets in the composite. Thus, solution blending offers a promising approach to dispersing GO platelets into certain polymer matrix. Specifically, small molecule functionalization and grafting-to/from methods have been reported to achieve stable GO platelet suspensions prior to mixing with polymer matrix. Some techniques, including Lyophilizations methods [66], phase transfer techniques [67], and surfactants [68] have been employed to facilitate solution blending of graphene-polymer nanocomposites. Nevertheless, surfactants may deteriorate composite properties. For example, the matrix-filler interfa-

cial thermal resistance in SWNT/polymer nanocomposites was increased by employing surfactants [69].

Melt mixing

Melt mixing technique utilizes a high temperature and shear forces to disperse the fillers in the polymer matrix. This process prevents the use of toxic solvents. Furthermore, compared with solution blending, melt mixing is often believed to be more cost effective. For graphene-polymer nanocomposites, the high temperature liquefies the polymer phase and allows easy dispersion or intercalation of GO platelets. However, the melt mixing is less effective in dispersing graphene sheets compared to solvent blending or in situ polymerization due to the increased viscosity at a high filler loading. The process can be applicable to both polar and non-polar polymers. Various graphene-based nanocomposites such as, exfoliated graphite-PMMA, graphene-polypropylene (PP), GO-poly (ethylene-2, 6-naphthalate) (PEN) and graphene-polycarbonate, can be fabricated by this technique. Even though the utility of graphene nanofiller is constrained by the low throughput of chemically reduced graphene in the melt mixing process, graphene production in bulk quantity in thermal reduction can be an appropriate choice for industrial scale production. However, the loss of the functional group in thermal reduction may be an obstacle in obtaining homogeneous dispersion in polymeric matrix melts especially in non-polar polymers.

In situ polymerization

This fabrication technique starts with mixing of filler in neat monomer (or multiple monomers), followed by polymerization in the presence of the dispersed filler. Then, precipitation/extraction or solution casting follows to generate samples for testing. In situ polymerization methods have produced composites with covalent crosslink between the matrix and filler. In addition, in situ polymerization has also produced non-covalent composites of a variety of polymers, such as poly (ethylene), PMMA and poly (pyrrole).

Unlike solution blending or melt mixing techniques, in situ polymerization technique achieves a high level of dispersion of graphene-based filler without prior exfoliation. It has been reported that monomer is intercalated between the layers of graphite or GO, followed by polymerization to separate the layers. This technique has been widely investigated for graphite or GO-derived polymer nanocomposites. For example, graphite can be intercalated by an alkali metal and a monomer, followed by polymerization initiated by thenegatively charged graphene sheets [70]. Although the polymerization may exfoliate the graphite nanoplatelets (GNPs), single-layer graphene platelets were not observed. TEM observation showed 3.6 nm thickness of graphene platelets with relatively low aspect ratio of about 30 dispersed in the PE matrix [71].

3.2. Fundamental properties

Mechanical properties

Higher mechanical properties of graphene sheets have attracted increasing attention worldwide. Similar to other composites, the mechanical properties depend on the

concentration, aspect ratio and distribution of the nanofiller in the matrix and the interface bonding. For example, at a nanofiller weight fraction of $0.1 \pm 0.002\%$, the graphene-epoxy nanocomposites show noticeable enhancement in the mechanical properties [3-5]. The Young's modulus, fracture strength of the nanocomposites are about $\sim 31\%$ and $\sim 40\%$ greater than the pristine epoxy, more efficient than the composites reinforced by multi-walled CNTs. The increase in fracture strength of the nanocomposites (graphene-PS) with $0.9 \text{ wt}\%$ graphene sheets is attributed to effective load transfer between the graphene layers and polymer matrix [72].

Besides simple reinforcing effects (Young's modulus and fracture strength), improvements in fracture toughness, fatigue strength and buckling resistance have also been reported in graphene-polymer nanocomposites [3,5,73-75]. For example, in situ polymerized graphene-epoxy nanocomposites show much higher buckling strength, fracture energy and fatigue strength than single- or multi-walled carbon nanotube-epoxy nanocomposites. However, the underlying strengthening and toughening mechanisms are still not well understood. Several factors, such as interfacial adhesion, spatial distribution and alignment of graphene nanofiller are considered to be crucial for effective reinforcement in the nanocomposites. Benefiting from improved interfacial adhesion, 76% and 62% the increase in elastic modulus and strength were achieved in the $0.7 \text{ wt}\%$ GO-PVA nanocomposite, respectively [76]. It was reported that the elastic modulus and fracture strength of Nylon-6 can be greatly improved by adding only $0.1 \text{ wt}\%$ GO [77]. The covalent bonding formed between the filler and matrix is attributed to the improved mechanical properties in the epoxy and polyurethane with GO-derived fillers [78-80]. Polymer nanocomposites with low loadings of functionalized graphene sheets (FGS) were reported to have a large shift in the glass transition temperature T_g [64]. In FGS-poly (acrylonitrile) nanocomposite, the shift in T_g is over 40°C when adding $1 \text{ wt}\%$ FGS filler loading. This behaviour can be attributed to the altered mobility of polymer chains at the filler-matrix interfaces [81,82]. Generally, a weak filler-matrix interface can constrain the chain mobility and thus increase the T_g .

Electrical properties

One of the most fascinating properties of graphene is its excellent electrical conductivity. When used as fillers in an insulating polymer matrix, conductive graphene may greatly improve the electrical conductivity of the composite. When the added graphene loading exceeds the electrical percolation threshold, a conductive network is expected in the polymer matrix. The conductivity σ_c as a function of filler loading can be described using a simple power-law expression, i.e.,

$$\sigma_c = \sigma_f (\phi - \phi_c)^t \quad (4)$$

where ϕ is the filler volume fraction; ϕ_c is the percolation threshold; σ_f is the filler conductivity, and t is a scaling exponent. The overall electrical performance is dependent on the processing and dispersion, aggregation and alignment of the filler. The intrinsic characteristics of the filler such as aspect ratio and morphology also play a role in dictating the conductivity. The inter-sheet junction formed may affect the conductivity as well.

A high level of dispersion may not necessarily promote the onset of electrical percolation [83]. The polymer reason is a thin layer of polymer may coat on the well-dispersed fillers and prevent direct the formation of a conductive network. In fact, the lowest electrical percolation threshold for graphene-polymer nanocomposites was reported for the nanocomposite with heterogeneously dispersed graphene (about 0.15 wt %) [84]. For example, compression moulded polycarbonate and GO-polyester nanocomposites with aligned platelets showed an increased percolation threshold that is about twice as high as the annealed samples with randomly oriented platelets [85,86]. Therefore, slight aggregation of the filler may lower the percolation threshold and improve the electrical conductivity of these nanocomposites [87]. Both theoretical analysis [88,89] and experiments demonstrated that the electrical conductivity of the nanocomposites correlates strongly with the aspect ratio of the platelets and higher aspect ratio leads to a higher conductivity. On the other hand, wrinkled, folded, or other non-flat morphologies may increase the electrical percolation threshold [90].

Thermal properties

The exceptional thermal properties of graphene have been used to improve the thermal stability and conductivity in nanocomposites. The 2D geometry of graphene-base materials may offer lower interfacial thermal resistance and thus provide higher thermal conductivity in the nanocomposites. The 2D geometry of graphene also introduces anisotropy into the thermal conductivity of graphene-polymer nanocomposites. For instance, the measured in-plane thermal conductivity is as much as ten times higher than the cross-plane conductivity [91]. Generally, thermal conductivity in nanocomposites can be analysed by percolation theory. Since phonons are the major mode of thermal conduction in amorphous polymers, covalent bonding between the filler and matrix can reduce phonon scattering at the filler-matrix interface, and subsequently enhance the thermal conductivity of nanocomposites [92]. In recent research, significant enhancements in thermal conductivity have been achieved in graphene-epoxy nanocomposites, with conductivities increasing to 3~6 W/mK from 0.2 W/mK for neat epoxy. However, such significant improvement often needs a high filler loading, about 20 wt% and even higher. Some research has also reported improvement in thermal stability of graphene-polymer nanocomposites [93,94]. Furthermore, the negative coefficient of thermal expansion (CTE) [95] and high surface of graphene can lower the CTE of polymer matrix [96]. For instance, the CTE of a GO-epoxy nanocomposite with 5% filler loading decreases by nearly 32% for temperature below the polymer glass transition Temperature (T_g) [97].

4. Structure-property relationship

4.1. Microstructure effect

TEM and wide-angle X-ray scattering (WAXS), are often utilized to examine the dispersion of graphene fillers in composites. Sometimes, the morphological features of dispersed fillers can be missed out due to the tiny platelet thickness and intensity scattering. Recently, small-angle X-ray scattering (SAXS) and ultra-small-angle X-ray scattering (USAXS) have been increasingly used to examine the aggregation of filler at large material length scale.

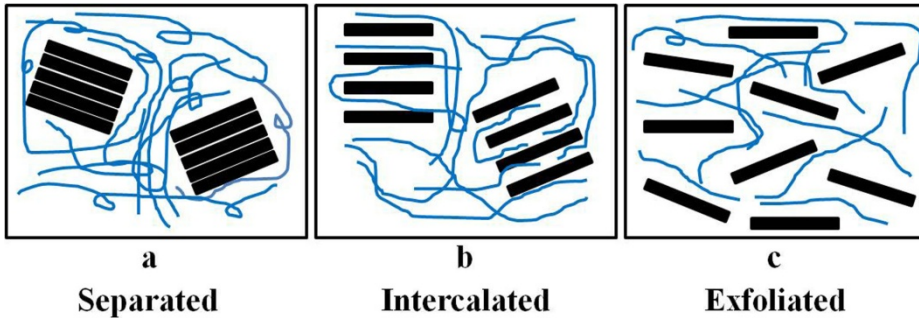


Figure 5. Filler dispersion in graphene-based nanocomposites: (a) separated, (b) intercalated, and (c) exfoliated phases.

In GO-derived and GNP-polymer nanocomposites, the fillers can exist in different forms such as stacked, intercalated or exfoliated, as shown in Figure 5. As compared with the separated phase, increased interlayer spacing (in the order of few nanometres) can be achieved in the intercalated structures. In the exfoliated structure, exfoliated platelets have the largest interfacial contact with the polymer matrix, generally ideal for improvement of various properties of the composites. Due to increased interaction with the polymer matrix, exfoliated phase normally has a curved shape when embedded into a polymer matrix. The rumpled shape of filler then can result in mechanical interlocking, which is one of the possible strengthening mechanisms. However, low modulus was also observed in the composite with wrinkled platelets [6]. The material processing methods can also influence the microstructure in nanocomposites. Randomly oriented exfoliated platelets can be achieved using solution blending or in situ polymerization [78]. Platelet restacking or incomplete exfoliation can also result in lower modulus due to decreased aspect ratio.

4.2. Interfacial behaviour

Although graphene-polymer nanocomposites exhibit excellent mechanical properties, the underlying strengthening and toughening mechanisms have not been well understood. Generally, it is believed that interfacial adhesion plays a key role in determining the improvements in mechanical properties of graphene-polymer nanocomposites. Low interfacial adhesion may lead to lower load transfer between the filler and matrix. Both AFM and Raman spectroscopy [98,99] can be utilized to measure the graphene-polymer interfacial adhesion. Raman spectra and their Raman bands were found to shift with stress, which enables stress-transfer to be monitored between the matrix and reinforcing phase. Moreover, a universal calibration has been established between the rate of shift of the G' band with strain [100]. Recently, interfacial shear stress [98] and effective Young's modulus [101] were successfully determined using Raman spectroscopy. The relationship between matrix strain ϵ_m and strain in the graphene flakes ϵ_c can be described by

$$\varepsilon_f = \varepsilon_m \left[1 - \frac{\cosh\left(\frac{ns \frac{x}{l}}{2}\right)}{\cosh\left(\frac{ns}{2}\right)} \right] \quad (5)$$

$$n = \sqrt{\frac{2G_m}{E_f}} \quad (6)$$

where n and G_m is the matrix shear modulus, E_f is the Young's modulus of the graphene filler. The variation of shear stress τ_i , at the graphene-polymer interface is given by

$$\tau_i = nE_f\varepsilon_m \frac{\sinh\left(\frac{ns \frac{l}{x}}{2}\right)}{\cosh\left(\frac{ns}{2}\right)} \quad (7)$$

Corresponding to $\varepsilon_m=0.4\%$, there is a good agreement between the measured and predicted (Equation 5) variation of fibre strain with position on the monolayer, validating the use of the shear lag analysis. At $\varepsilon_m=0.6\%$, however, the interface failure occurs between the filler and polymer and stress transfer is taking place through interfacial friction. The interfacial shear stress (ISS) between graphene and polymer is determined in the range of $\sim 0.3-0.8$ MPa, much lower than that between CNTs and polymer ($\sim 20-40$ MPa). The low ISS was attributed to the poor interface adhesion.

Raman spectroscopy analysis [98,102] confirmed the reinforcement effect of graphene and its dependence with crystallographic orientations and the layer number of graphene. It is demonstrated that monolayer or bilayer graphene has better load transfer than tri-layer or multi-layer [103]. Without compromising an even dispersion, higher filler loading is easy to achieve with multilayer graphene. There is therefore a balance in design of graphene-polymer nanocomposites between a higher filler loading and decreased load transfer as the number of layers in graphene filler increases. Raman G-band analysis suggested that load transfer at the GPL-PDMS interface is more effective in comparison to that along single wall carbon nanotube/PDMS interface [7]. In terms of loading mode, it is interesting to note that the GPL fillers went into compression under tensile loading and vice versa. Up to now, interface load transfer, mechanical interlocking caused by wrinkled surface and defects in graphene are main factor in controlling the reinforcement mechanisms. Due to the complex interactions between graphene, functional groups attached and the polymer, controversial results are often observed in the load transfer analysis. Further theoretical and numerical analysis is much needed.

5. Conclusion

In summary, the interesting properties of graphene and its composites mentioned above have led to the exploration of numerous applications such as transistors, chemical and biosensors, energy storage devices, nanoelectro-mechanical systems and others, just as the research

community has done with carbon nanotubes previously. The past decade has witnessed the rapid growth of carbon-based nanotechnology. Further research in the area will assist the development of next generation graphene based composites and hybrid materials.

Author details

Mingchao Wang, Cheng Yan and Lin Ma

School of Chemistry, Physics and Mechanical Engineering, Science and Engineering Faculty, Queensland University of Technology, Brisbane, Australia

6. References

- [1] Novoselov KS, Geim AK, Morozov SV, Jiang D, Zhang Y, Dubonos SV, Grigorieva IV, Firsov AA, *Science*. 306 (2004).
<http://www.sciencemag.org/content/306/5696/666.abstract>.
- [2] Stankovich S, Dikin DA, Dommett GHB, Kohlhaas KM, Zimney EJ, Stach EA, Piner RD, Nguyen ST, Ruoff RS, *Nature*. 442 (2006).
<http://dx.doi.org/10.1038/nature04969>.
- [3] Rafiee MA, Rafiee J, Wang Z, Song H, Yu Z-Z, Koratkar N, *ACS Nano*. 3 (2009).
<http://dx.doi.org/10.1021/nn9010472>.
- [4] Rafiee MA, Lu W, Thomas AV, Zandiatashbar A, Rafiee J, Tour JM, Koratkar NA, *ACS Nano*. 4 (2010).
<http://dx.doi.org/10.1021/nn102529n>.
- [5] Rafiee MA, Rafiee J, Srivastava I, Wang Z, Song HH, Yu ZZ, Koratkar N, *Small*. 6 (2010).
<http://dx.doi.org/10.1002/smll.200901480>.
- [6] Wakabayashi K, Pierre C, Dikin DA, Ruoff RS, Ramanathan T, Brinson LC, Torkelson JM, *Macromolecules*. 41 (2008).
<http://dx.doi.org/10.1021/ma071687b>.
- [7] Srivastava I, Mehta RJ, Yu Z-Z, Schadler L, Koratkar N, *Appl. Phys. Lett.* 98 (2011).
<http://link.aip.org/link/?APL/98/063102/1>.
- [8] Lee C, Wei X, Kysar JW, Hone J, *Science*. 321 (2008).
<http://www.sciencemag.org/content/321/5887/385.abstract>.
- [9] Scharfenberg S, Rocklin DZ, Chialvo C, Weaver RL, Goldbart PM, Mason N, *Appl. Phys. Lett.* 98 (2011).
<http://link.aip.org/link/?APL/98/091908/1>.
- [10] Zhao H, Min K, Aluru NR, *Nano Lett.* 9 (2009).
<http://dx.doi.org/10.1021/nl901448z>.
- [11] Wang MC, Yan C, Ma L, Hu N, Chen MW, *Comp. Mater. Sci.* 54 (2012).
<http://www.sciencedirect.com/science/article/pii/S0927025611006033>.
- [12] Zhao H, Aluru NR, *J. Appl. Phys.* 108 (2010).
<http://link.aip.org/link/?JAP/108/064321/1>.
- [13] Tsoukleri G, Parthenios J, Papagelis K, Jalil R, Ferrari AC, Geim AK, Novoselov KS, Galiotis C, *Small*. 5 (2009).

- <http://dx.doi.org/10.1002/sml.200900802>.
- [14] Lee C, Wei X, Li Q, Carpick R, Kysar JW, Hone J, *physica status solidi (b)*. 246 (2009).
<http://dx.doi.org/10.1002/pssb.200982329>.
- [15] Koenig SP, Boddeti NG, Dunn ML, Bunch JS, *Nat Nano*. 6 (2011).
<http://dx.doi.org/10.1038/nnano.2011.123>.
- [16] Zhang Y, Tan Y-W, Stormer HL, Kim P, *Nature*. 438 (2005).
<http://dx.doi.org/10.1038/nature04235>.
- [17] Novoselov KS, Jiang Z, Zhang Y, Morozov SV, Stormer HL, Zeitler U, Maan JC, Boebinger GS, Kim P, Geim AK, *Science*. 315 (2007).
<http://www.sciencemag.org/content/315/5817/1379.abstract>.
- [18] Geim AK, Novoselov KS, *Nat. Mater*. 6 (2007).
<http://dx.doi.org/10.1038/nmat1849>.
- [19] Somani PR, Somani SP, Umeno M, *Chem. Phys. Lett*. 430 (2006).
<http://www.sciencedirect.com/science/article/pii/S0009261406009018>.
- [20] Bae S, Kim H, Lee Y, Xu X, Park J-S, Zheng Y, Balakrishnan J, Lei T, Ri Kim H, Song YI, Kim Y-J, Kim KS, Ozyilmaz B, Ahn J-H, Hong BH, Iijima S, *Nat Nano*. 5 (2010).
<http://dx.doi.org/10.1038/nnano.2010.132>.
- [21] Kim KS, Zhao Y, Jang H, Lee SY, Kim JM, Kim KS, Ahn J-H, Kim P, Choi J-Y, Hong BH, *Nature*. 457 (2009).
<http://dx.doi.org/10.1038/nature07719>.
- [22] Berger C, Song Z, Li T, Li X, Ogbazghi AY, Feng R, Dai Z, Marchenkov AN, Conrad EH, First PN, de Heer WA, *The Journal of Physical Chemistry B*. 108 (2004).
<http://dx.doi.org/10.1021/jp040650f>.
- [23] Berger C, Song Z, Li X, Wu X, Brown N, Naud C, Mayou D, Li T, Hass J, Marchenkov AN, Conrad EH, First PN, de Heer WA, *Science*. 312 (2006).
<http://www.sciencemag.org/content/312/5777/1191.abstract>.
- [24] Zheng Q, Geng Y, Wang S, Li Z, Kim J-K, *Carbon*. 48 (2010).
<http://www.sciencedirect.com/science/article/B6TWD-50NBNTH-1/2/f9d91c8358333a00160e505b972e0cd3>.
- [25] Pei QX, Zhang YW, Shenoy VB, *Carbon*. 48 (2010).
<http://www.sciencedirect.com/science/article/B6TWD-4XNF8DY-3/2/d59770660b4ae737f9385b89c3439a0c>.
- [26] OuYang F, Huang B, Li Z, Xiao J, Wang H, Xu H, *J. Phys. Chem. C*. 112 (2008).
<http://dx.doi.org/10.1021/jp710547x>.
- [27] Lahiri J, Lin Y, Bozkurt P, Oleynik II, Batzill M, *Nat Nano*. 5 (2010).
<http://dx.doi.org/10.1038/nnano.2010.53>.
- [28] Stone AJ, Wales DJ, *Chem. Phys. Lett*. 128 (1986).
<http://www.sciencedirect.com/science/article/pii/0009261486806613>.
- [29] Meyer JC, Kisielowski C, Erni R, Rossell MD, Crommie MF, Zettl A, *Nano Lett*. 8 (2008).
<http://dx.doi.org/10.1021/nl801386m>.
- [30] Li L, Reich S, Robertson J, *Phys. Rev. B*. 72 (2005).
<http://link.aps.org/doi/10.1103/PhysRevB.72.184109>.
- [31] Ma J, Alfè D, Michaelides A, Wang E, *Phys. Rev. B*. 80 (2009).

- <http://link.aps.org/doi/10.1103/PhysRevB.80.033407>.
- [32] Ertekin E, Chrzan DC, Daw MS, Phys. Rev. B. 79 (2009).
<http://link.aps.org/doi/10.1103/PhysRevB.79.155421>.
- [33] Gass MH, Bangert U, Bleloch AL, Wang P, Nair RR, Geim AK, Nat Nano. 3 (2008).
<http://dx.doi.org/10.1038/nnano.2008.280>.
- [34] Ugeda MM, Brihuega I, Guinea F, Gómez-Rodríguez JM, Phys. Rev. Lett. 104 (2010).
<http://link.aps.org/doi/10.1103/PhysRevLett.104.096804>.
- [35] Krasheninnikov AV, Lehtinen PO, Foster AS, Nieminen RM, Chem. Phys. Lett. 418 (2006).
<http://www.sciencedirect.com/science/article/pii/S0009261405016544>.
- [36] Kotakoski J, Krasheninnikov AV, Nordlund K, Phys. Rev. B. 74 (2006).
<http://link.aps.org/doi/10.1103/PhysRevB.74.245420>.
- [37] Banhart F, Kotakoski J, Krasheninnikov AV, ACS Nano. 5 (2010).
<http://dx.doi.org/10.1021/nn102598m>.
- [38] Coraux J, N`Diaye AT, Busse C, Michely T, Nano Lett. 8 (2008).
<http://dx.doi.org/10.1021/nl0728874>.
- [39] Cervenka J, Katsnelson MI, Flipse CFJ, Nat Phys. 5 (2009).
<http://dx.doi.org/10.1038/nphys1399>.
- [40] Yazyev OV, Louie SG, Phys. Rev. B. 81 (2010).
<http://link.aps.org/doi/10.1103/PhysRevB.81.195420>.
- [41] Mermin ND, Physical Review. 176 (1968).
<http://link.aps.org/doi/10.1103/PhysRev.176.250>.
- [42] Nelson DR, Peliti L, Journal De Physique. 48 (1987).
<http://hal.archives-ouvertes.fr/jpa-00210530/en/>.
- [43] Le Doussal P, Radzihovsky L, Phys. Rev. Lett. 69 (1992).
<http://link.aps.org/doi/10.1103/PhysRevLett.69.1209>.
- [44] Meyer JC, Geim AK, Katsnelson MI, Novoselov KS, Booth TJ, Roth S, Nature. 446 (2007).
<http://dx.doi.org/10.1038/nature05545>.
- [45] Li Z, Cheng Z, Wang R, Li Q, Fang Y, Nano Lett. 9 (2009).
<http://dx.doi.org/10.1021/nl901815u>.
- [46] Teng L, Model. Simul. Mater. Sc. 19 (2011).
<http://stacks.iop.org/0965-0393/19/i=5/a=054005>.
- [47] Fasolino A, Los JH, Katsnelson MI, Nature Materials. 6 (2007).
<http://www.nature.com/nmat/journal/v6/n11/full/nmat2011.html>.
- [48] Duan WH, Gong K, Wang Q, Carbon. 49 (2011).
<http://www.sciencedirect.com/science/article/pii/S0008622311002247>.
- [49] Xu Z, Buehler MJ, ACS Nano. 4 (2010).
<http://dx.doi.org/10.1021/nn100575k>.
- [50] Shenoy VB, Reddy CD, Ramasubramaniam A, Zhang YW, Phys. Rev. Lett. 101 (2008).
<http://link.aps.org/doi/10.1103/PhysRevLett.101.245501>.
- [51] Huang B, Liu M, Su N, Wu J, Duan W, Gu B-l, Liu F, Phys. Rev. Lett. 102 (2009).
<http://link.aps.org/doi/10.1103/PhysRevLett.102.166404>.
- [52] Bets KV, Yakobson BI, Nano Research. 2 (2009).

- <http://www.nanoarchive.org/8385/>.
- [53] Reddy CD, Ramasubramaniam A, Shenoy VB, Zhang Y-W, *Appl. Phys. Lett.* 94 (2009).
<http://link.aip.org/link/?APL/94/101904/1>
<http://dx.doi.org/10.1063/1.3094878>.
- [54] Pei QX, Zhang YW, Shenoy VB, *Nanotechnology.* 21 (2010).
<http://dx.doi.org/10.1088/0957-4484/21/11/115709>.
- [55] Ishigami M, Chen JH, Cullen WG, Fuhrer MS, Williams ED, *Nano Lett.* 7 (2007).
<http://dx.doi.org/10.1021/nl070613a>.
- [56] Stolyarova E, Rim KT, Ryu S, Maultzsch J, Kim P, Brus LE, Heinz TF, Hybertsen MS, Flynn GW, *P. Natl. Acad. Sci. USA.* 104 (2007).
<http://www.pnas.org/content/104/22/9209.abstract>.
- [57] Stoberl U, Wurstbauer U, Wegscheider W, Weiss D, Eroms J, *Appl. Phys. Lett.* 93 (2008).
<http://dx.doi.org/10.1063/1.2968310>.
- [58] Geringer V, Liebmann M, Echtermeyer T, Runte S, Schmidt M, Rückamp R, Lemme MC, Morgenstern M, *Phys. Rev. Lett.* 102 (2009).
<http://link.aps.org/doi/10.1103/PhysRevLett.102.076102>.
- [59] Teng L, Zhao Z, *J. Phys. D Appl. Phys.* 43 (2010).
<http://stacks.iop.org/0022-3727/43/i=7/a=075303>.
- [60] Zhang Z, Li T, *J. Appl. Phys.* 107 (2010).
<http://dx.doi.org/10.1063/1.3427551>.
- [61] Zhang Z, Li T, *J. Nanomater.* 2011 (2011).
<http://dx.doi.org/10.1155/2011/374018>.
- [62] Higginbotham AL, Lomeda JR, Morgan AB, Tour JM, *ACS Appl. Mater. Inter.* 1 (2009).
<http://dx.doi.org/10.1021/am900419m>.
- [63] Chen D, Zhu H, Liu T, *ACS Appl. Mater. Inter.* 2 (2010).
<http://dx.doi.org/10.1021/am1008437>.
- [64] Ramanathan T, Abdala AA, Stankovich S, Dikin DA, Herrera Alonso M, Piner RD, Adamson DH, Schniepp HC, Chen X, Ruoff RS, Nguyen ST, Aksay IA, Prud'Homme RK, Brinson LC, *Nat Nano.* 3 (2008).
<http://dx.doi.org/10.1038/nnano.2008.96>.
- [65] Xu Y, Hong W, Bai H, Li C, Shi G, *Carbon.* 47 (2009).
<http://www.sciencedirect.com/science/article/pii/S0008622309005296>.
- [66] Cao Y, Feng J, Wu P, *Carbon.* 48 (2010).
<http://www.sciencedirect.com/science/article/pii/S0008622310004549>.
- [67] Wei T, Luo G, Fan Z, Zheng C, Yan J, Yao C, Li W, Zhang C, *Carbon.* 47 (2009).
<http://www.sciencedirect.com/science/article/pii/S0008622309002565>.
- [68] Lee HB, Raghu AV, Yoon KS, Jeong HM, *J. Macromol. Sci. B.* 49 (2010).
<http://www.tandfonline.com/doi/abs/10.1080/00222341003603701>.
- [69] Bryning MB, Milkie DE, Islam MF, Kikkawa JM, Yodh AG, *Appl. Phys. Lett.* 87 (2005).
<http://dx.doi.org/10.1063/1.2103398>.
- [70] Shioyama H, *Synthetic Metals.* 114 (2000).
<http://www.sciencedirect.com/science/article/pii/S0379677900002228>.
- [71] Fim FdC, Guterres JM, Basso NRS, Galland GB, *J. Polym. Sci. Pol. Chem.* 48 (2010).

- <http://dx.doi.org/10.1002/pola.23822>.
- [72] Fang M, Wang K, Lu H, Yang Y, Nutt S, J. Mater. Chem. 19 (2009).
<http://dx.doi.org/10.1039/B908220D>.
- [73] Rafiee MA, Rafiee J, Yu ZZ, Koratkar N, Appl. Phys. Lett. 95 (2009).
http://apl.aip.org/applab/v95/i22/p223103_s1?isAuthorized=no.
- [74] Yavari F, Rafiee MA, Rafiee J, Yu ZZ, Koratkar N, ACS Appl. Mater. Inter. 2 (2010).
<http://dx.doi.org/10.1021/am100728r>.
- [75] Rafiq R, Cai D, Jin J, Song M, Carbon. 48 (2010).
<http://www.sciencedirect.com/science/article/pii/S0008622310005476>.
- [76] Liang J, Huang Y, Zhang L, Wang Y, Ma Y, Guo T, Chen Y, Adv. Funct. Mater. 19 (2009).
<http://dx.doi.org/10.1002/adfm.200801776>.
- [77] Xu Z, Gao C, Macromolecules. 43 (2010).
<http://dx.doi.org/10.1021/ma1009337>.
- [78] Kim H, Miura Y, Macosko CW, Chem. Mater. 22 (2010).
<http://dx.doi.org/10.1021/cm100477v>.
- [79] Lee YR, Raghu AV, Jeong HM, Kim BK, Macromol. Chem. Physic. 210 (2009).
<http://dx.doi.org/10.1002/macp.200900157>.
- [80] Miller SG, Bauer JL, Maryanski MJ, Heimann PJ, Barlow JP, Gosau J-M, Allred RE, Compos. Sci. Technol. 70 (2010).
<http://www.sciencedirect.com/science/article/pii/S0266353810000825>.
- [81] Bansal A, Yang H, Li C, Cho K, Benicewicz BC, Kumar SK, Schadler LS, Nat. Mater. 4 (2005).
<http://dx.doi.org/10.1038/nmat1447>.
- [82] Priestley RD, Ellison CJ, Broadbelt LJ, Torkelson JM, Science. 309 (2005).
<http://www.sciencemag.org/content/309/5733/456.abstract>.
- [83] Schaefer DW, Justice RS, Macromolecules. 40 (2007).
<http://dx.doi.org/10.1021/ma070356w>.
- [84] Pang H, Chen T, Zhang G, Zeng B, Li Z-M, Mater. Lett. 64 (2010).
<http://www.sciencedirect.com/science/article/pii/S0167577X10005379>.
- [85] Kim H, Macosko CW, Macromolecules. 41 (2008).
<http://dx.doi.org/10.1021/ma702385h>.
- [86] Kim H, Macosko CW, Polymer. 50 (2009).
<http://www.sciencedirect.com/science/article/pii/S0032386109004558>.
- [87] Bauhofer W, Kovacs JZ, Compos. Sci. Technol. 69 (2009).
<http://www.sciencedirect.com/science/article/pii/S026635380800239X>.
- [88] Hicks J, Behnam A, Ural A, Appl. Phys. Lett. 95 (2009).
<http://dx.doi.org/10.1063/1.3267079>.
- [89] Li J, Kim J-K, Compos. Sci. Technol. 67 (2007).
<http://www.sciencedirect.com/science/article/pii/S0266353806004386>.
- [90] Yi YB, Tawerghi E, Phys. Rev. E. 79 (2009).
<http://link.aps.org/doi/10.1103/PhysRevE.79.041134>.

- [91] Veca LM, Mezziani MJ, Wang W, Wang X, Lu F, Zhang P, Lin Y, Fee R, Connell JW, Sun Y-P, *Adv. Mater.* 21 (2009).
<http://dx.doi.org/10.1002/adma.200802317>.
- [92] Ganguli S, Roy AK, Anderson DP, *Carbon.* 46 (2008).
<http://www.sciencedirect.com/science/article/pii/S000862230800078X>.
- [93] Kim I-H, Jeong YG, *Journal of Polymer Science Part B: Polymer Physics.* 48 (2010).
<http://dx.doi.org/10.1002/polb.21956>.
- [94] Bao Q, Zhang H, Yang J-x, Wang S, Tang DY, Jose R, Ramakrishna S, Lim CT, Loh KP, *Adv. Funct. Mater.* 20 (2010).
<http://dx.doi.org/10.1002/adfm.200901658>.
- [95] Bao W, Miao F, Chen Z, Zhang H, Jang W, Dames C, Lau CN, *Nat Nano.* 4 (2009).
<http://dx.doi.org/10.1038/nnano.2009.191>.
- [96] Paul DR, Robeson LM, *Polymer.* 49 (2008).
<http://www.sciencedirect.com/science/article/pii/S0032386108003157>.
- [97] Wang S, Tambraparni M, Qiu J, Tipton J, Dean D, *Macromolecules.* 42 (2009).
<http://dx.doi.org/10.1021/ma900631c>.
- [98] Gong L, Kinloch IA, Young RJ, Riaz I, Jalil R, Novoselov KS, *Adv. Mater.* 22 (2010).
<http://onlinelibrary.wiley.com/doi/10.1002/adma.200904264/abstract>.
- [99] Kranbuehl DE, Cai M, Glover AJ, Schniepp HC, *J. Appl. Pol. Sci.* 122 (2011).
<http://dx.doi.org/10.1002/app.34787>.
- [100] Cooper CA, Young RJ, Halsall M, *Compos A Appl. Sci. Manu.* 32 (2001).
<http://www.sciencedirect.com/science/article/pii/S1359835X0000107X>.
- [101] Frank O, Tsoukleri G, Riaz I, Papagelis K, Parthenios J, Ferrari AC, Geim AK, Novoselov KS, Galiotis C, *Nat Commun.* 2 (2011).
<http://dx.doi.org/10.1038/ncomms1247>.
- [102] Young RJ, Gong L, Kinloch IA, Riaz I, Jalil R, Novoselov KS, *ACS Nano.* 5 (2011).
<http://pubs.acs.org/doi/abs/10.1021/nn2002079>.
- [103] Gong L, Young RJ, Kinloch IA, Riaz I, Jalil R, Novoselov KS, *ACS Nano.* (2012).
<http://dx.doi.org/10.1021/nn203917d>.